A MULTISCALE DAMAGE MODEL FOR THE MECHANICAL BEHAVIOUR OF CERAMIC MATRIX COMPOSITE MATERIALS

A. Coradi, G. Couégnat, E. Martin, F. Mahdi

Laboratoire des Composites ThermoStructuraux, (LCTS), Univ. de Bordeaux; CNRS; SAFRAN-SPS; CEA, 3 allée de la Boétie, 33600 Pessac, France
{coradi, couegnat, martin, mahdi} @lcts.u-bordeaux1.fr

Keywords: Multiscale analysis, Cohesive zone model, interfacial debonding, Ceramic Matrix Composite.

Abstract
The mechanical behavior and the damage development in ceramic matrix composites under uniaxial tension are investigated with a multiscale approach. Matrix cracking and interfacial debonding at the yarn scale and at the mesoscale are examined. Representative cells are meshed using tools specifically developed for modeling woven composite. A finite element analysis with cohesive zone models is proposed to describe the two damage mechanisms considered. Matrix cracking and interfacial debonding kinetics are evaluated by comparison with experimental data. It is shown that this multiscale procedure allows to analyze the damage development within the composite and to assess the influence of fracture properties and weaving on composite mechanical response.

1 Introduction
Ceramic matrix composites (CMC) have demonstrated attractive thermomechanical properties for structural applications at high temperature [1]. Those woven materials are particularized by a non linear mechanical behavior which results from development of crack networks at various scales. In spite of a complex microstructure, separation of length scale allows to distinguish the microscale (characterized by the fiber diameter about 15 microns) from the mesoscale (characterized by the thickness of the woven ply about 300 microns). The aim of this paper is to propose a multiscale approach for damage modeling in CMC. A numerical procedure is developed based on finite element analysis for modeling crack network evolution and the mechanical response under uniaxial extension. First the yarn scale is considered and then the woven composite scale is analyzed.

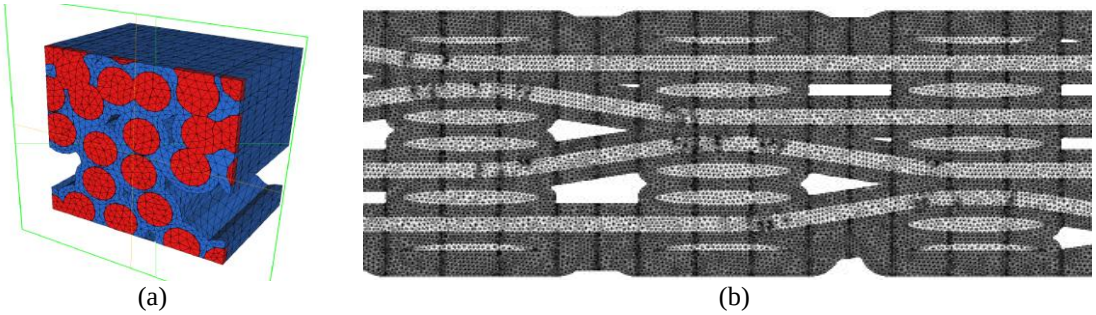

(a) (b)

Figure 1. Representative cells : a) yarn scale, b) mesoscale.

Representative cells of the composite at both scales are generated and meshed with the help of tools already developed in previous studies [2]. Figure 1 shows that the representative cells and volumes can be selected according to fiber volume fraction, matrix thickness, porosity or pattern of weaving.
The yarn scale is first considered for which damage occurs as matrix cracking and interfacial debonding. A cohesive zone model (CZM) is used to introduce the two damage mechanisms using representative cells of a minicomposite subjected to uniaxial extension. Matrix cracking and interfacial debonding kinetics are evaluated by comparing with experimental data obtained from tensile tests. An additional homogeneisation routine is devoted to estimate the effective properties of the damaged minicomposite. This procedure provides a constitutive damage law which is used to model the behavior of the yarns. For modeling damage at the mesoscale, a volume element of the CMC is meshed (Figure 1b) and CZMs are one more time required to analyze matrix cracking and interfacial debonding. This multiscale approach is illustrated by Figure 2.

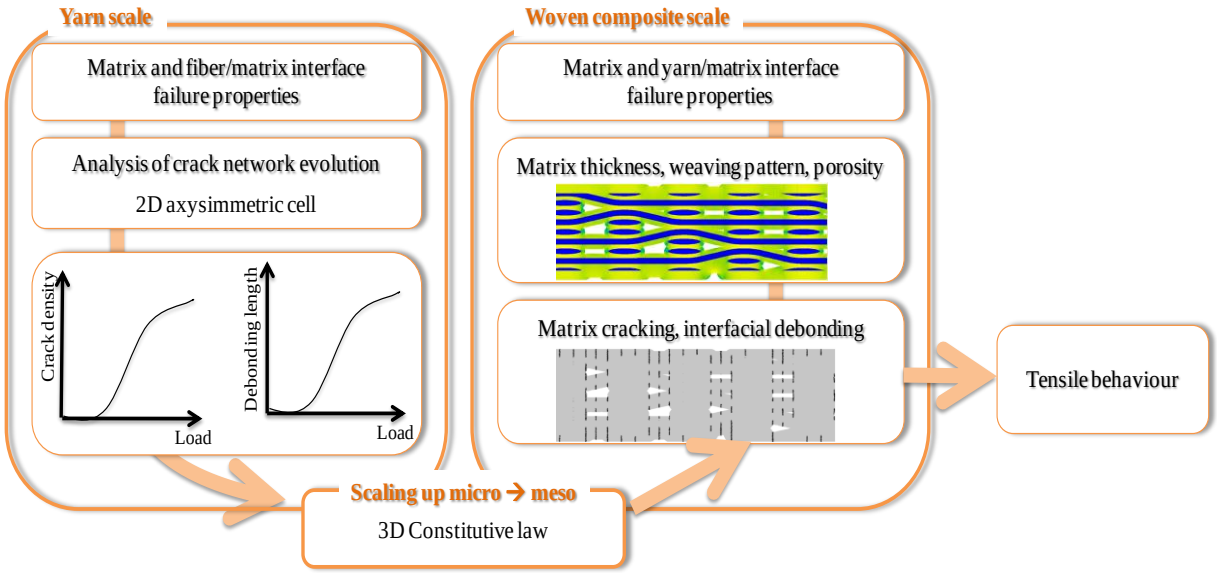

Figure 2. Multiscale damage modeling procedure.

2 Cohesive Zone Model for modeling matrix cracking and interfacial debonding

CZMs are chosen for modeling matrix cracking and interfacial debonding at yarn scale and mesoscale. They are characterized by a damage behavior law which links the relative displacements of the elements nodes to the local load.
For matrix cracking simulation, a bilinear model based on the Alfano-Crisfield approach [3] is used. Matrix cracking is controlled by the maximum stress σ_{max} (Figure 3a). Once this stress is reached, the stiffness decreases in the element which is stated broken when the relative normal displacement is δ_n. A parametrical study was preliminarily undertaken to select the appropriate values of the initial stiffness (depending on U_{0n}) and the maximum displacement δ_n.

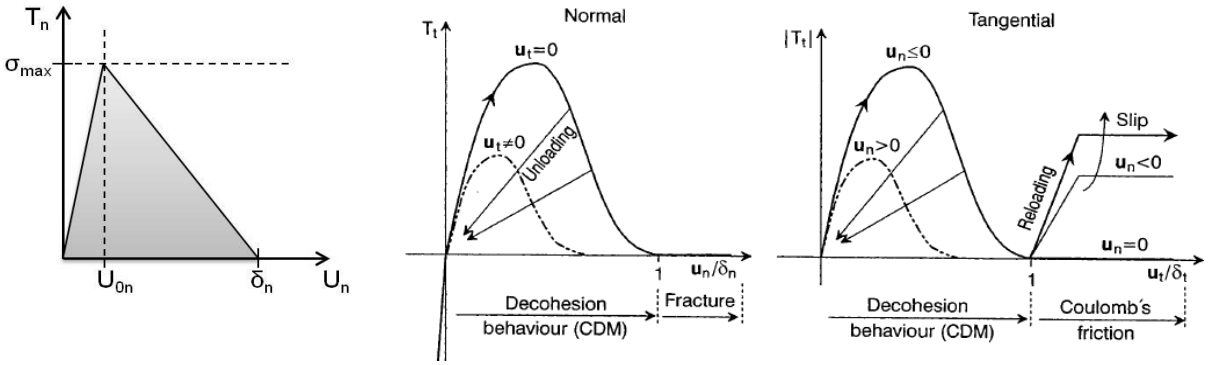

(a) Matrix cracking (b) Interfacial cracking

Figure 3. Cohesive zone model : a) matrix cracking, b) interfacial debonding. Figure 3a represents the normal stress $\mathbf{T_n}$ versus the relative normal displacement $\mathbf{U_n}$, governed by the maximum stress $\boldsymbol{\sigma_{max}}$ and displacement $\boldsymbol{\delta_n}$. The initial stiffness is set according to the displacement $\mathbf{U_{0n}}$. Figure 3b shows the Tvergaard-Needleman model used for interfacial debonding [5]. It represents the normal and tangential behavior that link the normal or tangential load $\mathbf{[T_n, T_t]}$ to the relative displacements $\mathbf{[u_n, u_t]}$. After the element is broken, the tangential stress depends on the friction coefficient and on the normal stress.

The Tvergaard-Needelman model [4] has been chosen for interfacial debonding. The model has been modified [5] so that sliding friction is allowed after the element is broken (Figure 3b). In this case, the interfacial stress is not zero but depends on the friction coefficient $\boldsymbol{\mu}$ and on the normal stress according to Coulomb friction law. Interfacial debonding is set by the fiber/matrix interfacial energy release rate $\mathbf{G_i^c}$ (mode II) which is defined by the area under the tangential behavior curve (Figure 3 b). The parameters for crack propagation in mode I are taken arbitrarily high so that failure for this opening mode cannot happen. Finally the properties used to model both damage mechanisms are $\boldsymbol{\sigma_{max}}$, $\mathbf{G_i^c}$ and $\boldsymbol{\mu}$.

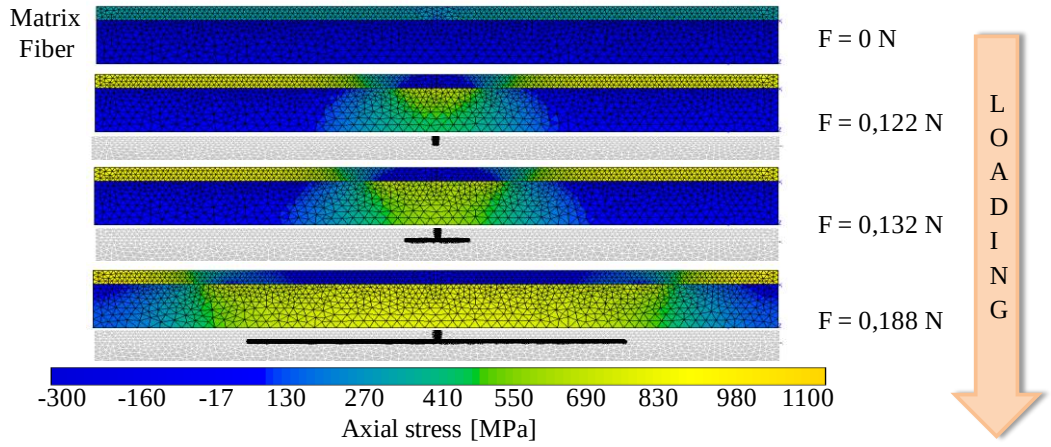

Figure 4. Evolution of matrix crack and deviation at the fiber/matrix interface during a uniaxial tension loading within an axisymmetric elementary cell. On the bottom diagrams the broken elements are represented which model damage growth. The upper figures show the axial stress distribution between matrix and fiber during loading and cracking evolution.

To illustrate damage modeling with such CZMs, first a representative elementary cell of the unidirectional composite is drawn and meshed. Figure 4 shows a representative axisymmetric cell of a silicium carbide (SiC) fiber coated with a SiC matrix. Interface elements with no thickness have been introduced for modeling a matrix crack in the middle of the cell and debonding between fiber and matrix. Then the previously mentioned CZMs are allocated to

these interface elements. A uniaxial loading is applied and the evolution of crack path is detailed. Elastic properties of fiber and matrix material, cell dimensions and failure properties chosen for this simulation are given in the Table 1 of the Appendix. Residual stresses which result from the elaboration phase at high temperature are taken into account. This simulation is performed with the cohesive model properties σ_{max} = 800 MPa and G_i^c = 4.2 J.m^{-2}. The matrix crack is first initiated and is instantly deflected at the fiber/matrix interface. At the same time, the axial stress is unloaded from the matrix to the fiber in the vicinity of cracks. Then the more the cell is loaded, the more the debonding propagates and the longer is the unloading distance. This damage evolution induces a loss of stiffness.

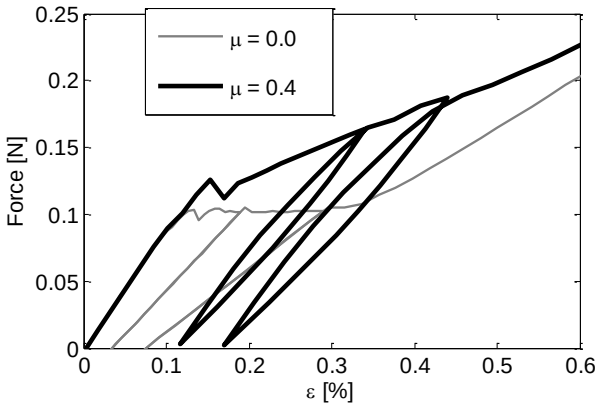

Figure 5. Force/strain curve of simulated tensile test with load cycles, where sliding at the interface is considered with or without friction (μ=0.4 or μ=0).

The simulated force/strain response indicates that a linear behavior is obtained until the matrix crack is initiated (Figure 5). Then interfacial debonding grows under imposed displacement. As illustrated by Figure 5, sliding friction is shown to provide shorter debonding length as well as larger applied force for the same displacement. The proposed model allows simulation of loading/unloading cycles. Hysteresis loops and residual strain depend on damage and on the friction coefficient value.

3 Non linear response and damage kinetics for yarns

The proposed model is used to describe the non-linear tensile response of SiC/SiC minicomposite and damage kinetics based on experimental data. A previous study [6] provides tensile force-displacement curves and matrix crack density at failure for SiC/SiC minicomposites with various fiber and matrix volume fractions. A representative axisymmetric cell unit consisting of a fiber coated with matrix is meshed. Numerous interface elements are periodically introduced in the matrix along the elementary cell length.

The first step of the proposed method needs to allocate maximum stress value $\boldsymbol{\sigma_{max}}$ to each CZM so that the cracking process matches experiment. A power law was found an appropriate model for linking the maximum stress $\boldsymbol{\sigma_{max}}$ to the matrix crack density $\boldsymbol{\rho}$. As shown in Figure 6, the identified power law allows to model matrix crack kinetics which is here compared with the experimental data obtained from acoustic emission and microscopic observations. Interfacial debonding develops with loading and slows down matrix cracking.

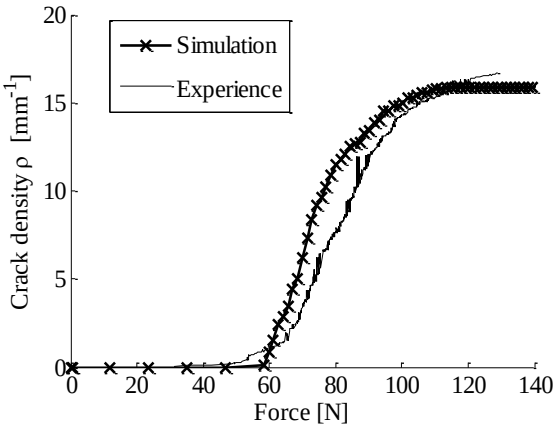

Figure 6. Matrix crack kinetics obtained with experimental data using acoustic emission for a tensile test on a SiC/SiC minicomposite [5]. Comparison is done with the simulated curve where an identified power law links the maximum stress σ_{max} to matrix crack density.

Then values of the interfacial energy release rate and friction coefficient are adjusted to fit the simulated force/strain curve with experimental data. It was found that the friction coefficient is a significant factor in tensile test response and that the interface failure energy must be adjusted to allow interface debonding to happen. The simulation plot in Figure 7 is obtained with the interfacial energy release rate $G_i^c = 6\ J.m^{-2}$ and a high value of the friction coefficient $\mu = 1.7$.

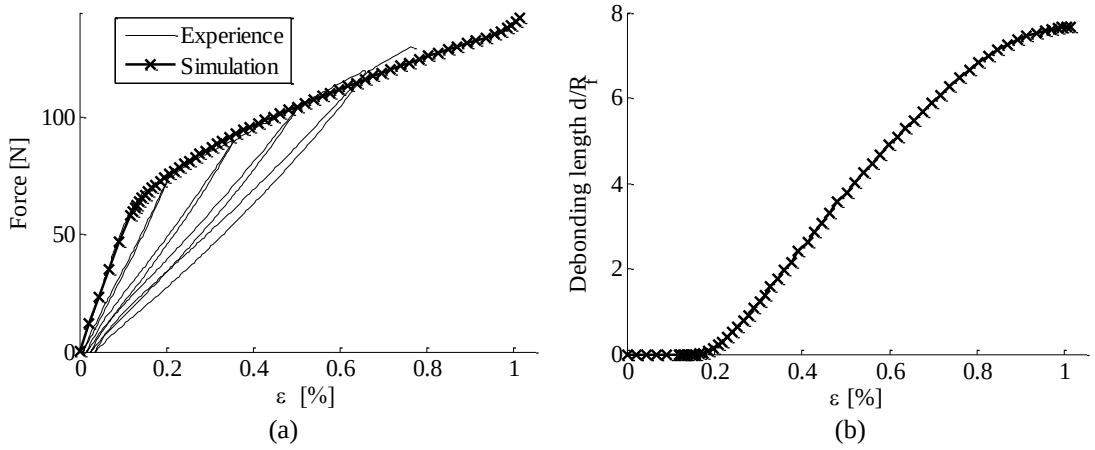

Figure 7. (a) Experimental Force/strain curve [5] compared to simulation. (b) Average debonding length related to each matrix crack normalized by fiber radius versus the applied strain.

Matrix crack density ρ and interfacial debonding length d can thus be evaluated as a function of the applied axial strain ε (Figure 7). To complete this procedure, an additional finite element calculation is used to model the evolution of the elastic properties in every direction (axial and transverse) relative to the two damage variables (ρ, d). For this purpose, a 3D representative volume (Figure 1a) is used in which matrix and interfacial cracks are inserted. The stiffness matrix $[C]$ can thus be evaluated as a function of (ρ, d). Finally a yarn damage law is formed by combining both $[C(\rho,d)]$ and the damage kinetics $\rho(\varepsilon)$ and $d(\varepsilon)$. This procedure provides a scaling up tool for modeling damage within longitudinal yarns at the mesoscale.

4 Woven composite damage modeling

The damage mechanisms considered at the mesoscale include matrix cracking and interfacial debonding between matrix and yarns. A bidimensional mesh representative of the woven composite is generated and the CZMs previously described are used. Matrix cracks are supposed to be oriented at right angles to the loading direction and interface elements with CZMs are introduced regularly inside the matrix part (Figure 1b) as well as at the interface between matrix and yarns for debonding modeling. Matrix properties are given in Table 1 and the elastic properties of the yarns are deduced from the previous study. The matrix maximum stress σ_{max} that leads to crack initiation is set to $\sigma_{max} = 400$ MPa.

Figure 8 shows that the number of matrix cracks increases with tension loading. The perfect bonding case is presented. The first cracks are initiated from the composite edge where high stress concentration is observed (Figure 8). Porosities generate others stress concentration areas that induce further matrix cracks. The modeled crack network evolution is well consistent with experimental observations. Then other cracks start elsewhere after the maximum stress is reached and the cracking process slows down. The corresponding matrix cracks kinetics is presented in Figure 9b.

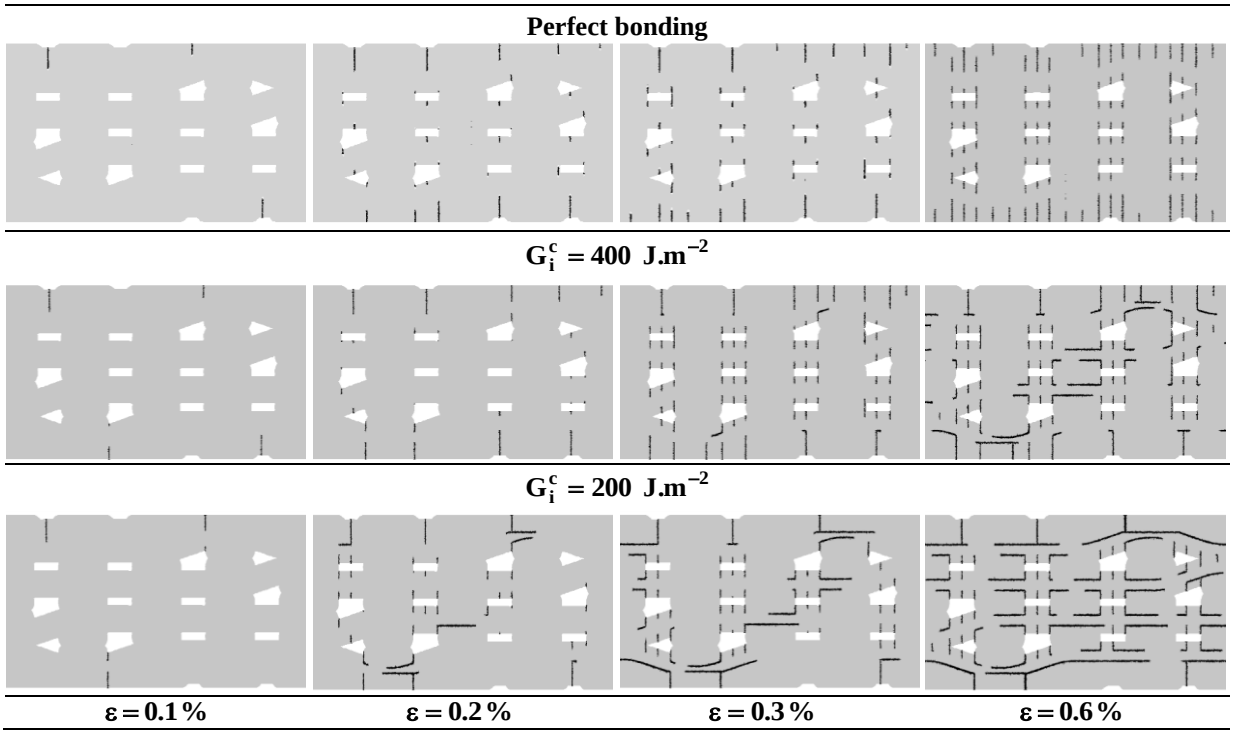

Figure 8. Matrix cracking and interfacial debonding progress versus the applied strain ε (the loading axis is horizontal). Comparison is done between the perfect bonding case and simulations using two values of the interfacial energy release rate G_i^c.

Interface debonding between yarns and matrix at this scale is controlled by the interfacial energy release rate G_i^c. Debonding initiates when matrix cracks reach an interface between the matrix and a yarn. The weaker is the interfacial fracture energy, the more the interfacial debonding growth (Figure 8). It is shown that debonding allows stress unloading within the matrix which slows down matrix crack progress from the composite edge. At the end of loading, the number of matrix cracks (Figure 9b) is saturated and depends on the interfacial energy G_i^c. Furthermore, debonding induces stress reloading which promotes matrix cracking

in the inner part of the composite. This mechanism explains that before saturation the number of matrix cracks increases for $\mathbf{G_i^c = 400\ J.m^{-2}}$ as illustrated in Figure 9b.

The corresponding stress/strain curve is given by Figure 9a. The elastic limit corresponds to the initiation of the first matrix cracks. Then crack progress induces a loss of stiffness until the number of cracks slows down, which is favored by interfacial debonding. Microscopic characterization enables to evaluate the number of matrix cracks within the woven composite but interfacial debonding in the inner composite is difficult to measure. Failure properties $(\boldsymbol{\sigma_{max}}, \mathbf{G_i^c})$ at the woven composite scale can be determined with experimental data using the evaluation of the number of matrix cracks and the stress/strain curve.

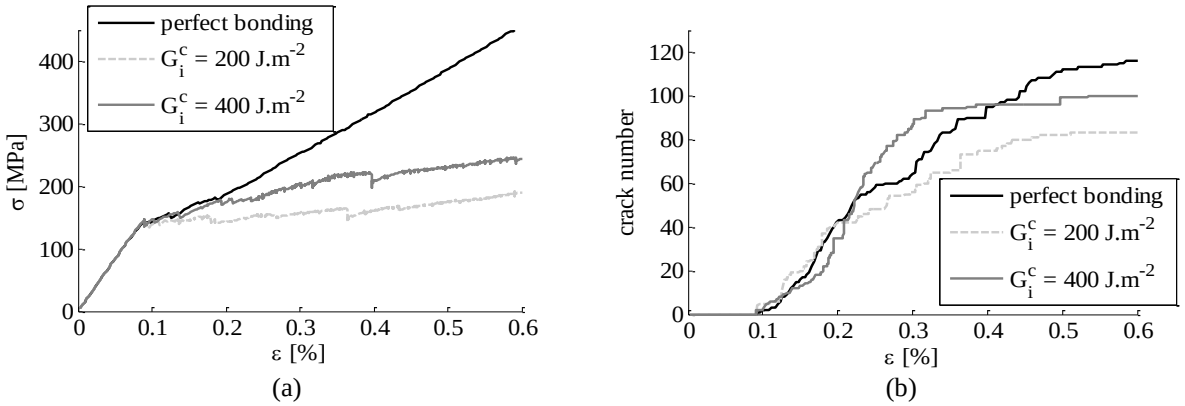

Figure 9. (a) Stress/strain curve simulated at mesoscale during matrix cracking and interfacial debonding progress. (b) Number of matrix cracks initiated within the 9.2 mm length cell according to the applied strain $\boldsymbol{\varepsilon}$. Comparison is made for three values of the interfacial energy release rate $\mathbf{G_i^c}$ which controls the debonding growth.

Then when the matrix crack network is saturated and the yarns alone support loading, the damage behaviour law previously developed for yarns allows to model damage progress within yarns. Figure 10 shows damage evolution within yarns according to the applied strain $\boldsymbol{\varepsilon}$ obtained with the 3D constitutive damage law mentioned in section 3. The simulation presented does not take into account matrix cracking and interfacial debonding at this scale. Damage is first initiated inside the yarns near the porosity where stress value is higher. The damaged behaviour law involves matrix crack and interfacial debonding that depend on the local axial strain. At the end of loading, inner yarn damage progress comes to uniformity until damage is saturated.

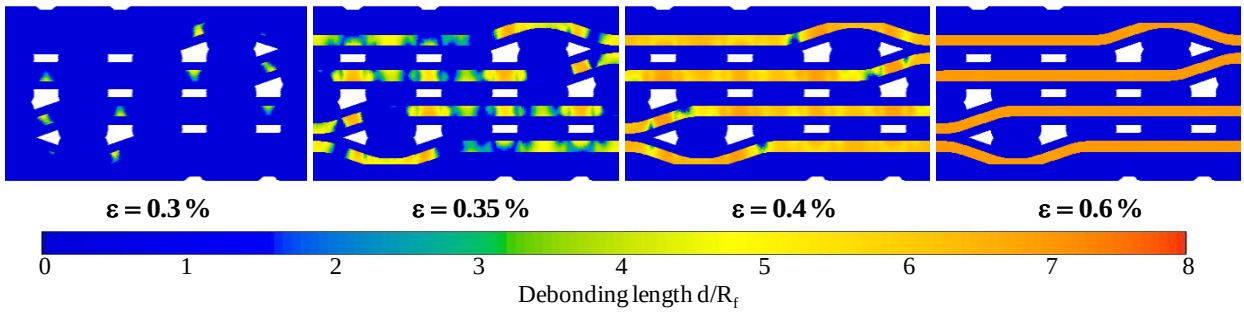

Figure 10. Damage evolution within the yarns obtained with the 3D constitutive law. Matrix crack and debonding is not considered for this simulation.

CZMs at yarn scale allow evaluating crack opening displacement according to loading. The yarn behaviour law developed is being enhanced for modeling crack opening displacement

within yarns at the woven composite scale. Others improvements will be added such as the mechanisms of transverse yarns cracking.

5 Conclusion

A multiscale damage procedure of CMC for analyzing matrix cracking and interfacial debonding within yarns and woven composite is proposed. The numerical analysis uses cohesive zone models which requires the following parameters : maximum stress σ_{max} for matrix crack initiation, energy release rate G_i^c and friction coefficient μ for debonding and sliding friction.

Damage kinetics is modeled at yarn scale based on the tensile test response of minicomposite. Failure properties (σ_{max}, G_i^c) and friction coefficient have been identified so that a good agreement is obtained. This model is included in a constitutive law used at mesoscale. Woven composite representative cell is meshed and matrix cracks are modeled with CZM so that the influence of weaving and porosity can be assessed.

On-going works consider crack opening displacement measured and modeled according to loading in the context of lifetime modeling. This procedure proposes a valuable method for understanding woven composite damage mechanisms and its influence on the mechanical response, thus providing a useful tool for the composite designer.

References

[1] Naslain R., Design, Preparation and properties of non-oxide CMCs for application in engines and nuclear reactors: an overview. *Compos. Sci. Technol*. **64**, pp.155-170 (2004).

[2] Couegnat G., Martin E., Lamon J., *Multiscale modelling of the mechanical behaviour of woven* composite *materials* in "Proceeding of *International Committee on Composite Materials-17"*, Edinburgh, United Kingdom, (2009).

[3] Alfano G., Crisfield M.A., Finite element interface models for delamination analysis of laminated composites: mechanical and computational issues. *Int. J. Numer. Meth. Engng*, **50**, pp. 1701-1736 (2001).

[4] Needleman A., A continuum model for void nucleation by inclusion debonding. *J. Appl. Mech*, **54**, pp. 525-531 (1996).

[5] Chaboche J.L., Girard R., Schaff A., Numerical analysis of composite systems by using interphase/interface models, *Computational Mechanics*, **20**, pp. 3-11 (1997).

[6] Etchart-Salas R., Jacques S., Coradi A., Martin E., *Elaboration and mechanical characterisation of unidirectional ceramic matrix composites* in "Proceeding of *Journées Nationales sur les Composites JNC 17"*, Poitiers, France, (2011).

Appendix

Fiber and matrix elastic properties as well as dimensions of the representative cell (minicomposite) used to set up cohesive zone model are given below.

R_m	10.5 μm	E_m	400 GPa	ν	0.2	α_m	4.6 10^{-6} °C	**L**	100 μm
R_f	8 μm	E_f	200 GPa	ν	0.2	α_f	2.9 10^{-6} °C	**ΔT**	-1000 °C

Table 1. Constituents properties of the studied representative cell with length **L**, (radius R_m and R_f, Young modulus E_m and E_f, same Poisson's ratio ν, expansion coefficient α_m and α_f respectively of matrix and fibers, temperature change **ΔT** after the composite processing).